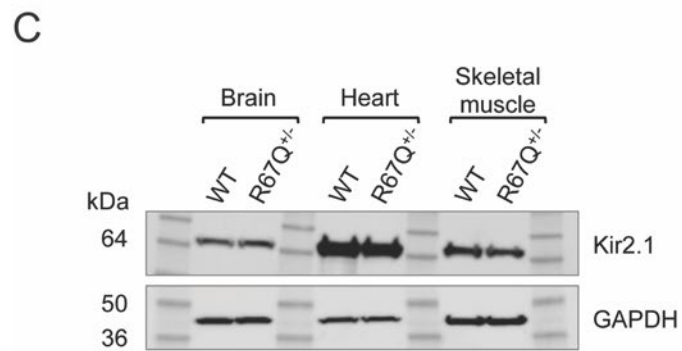
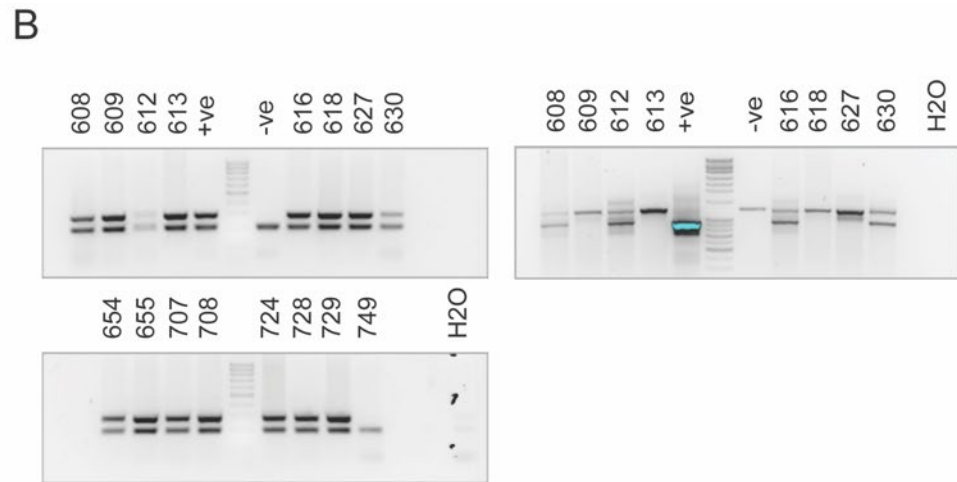
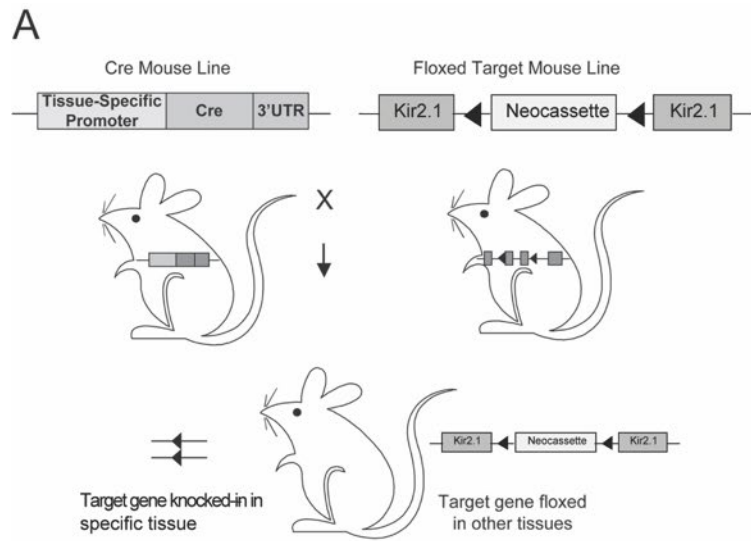


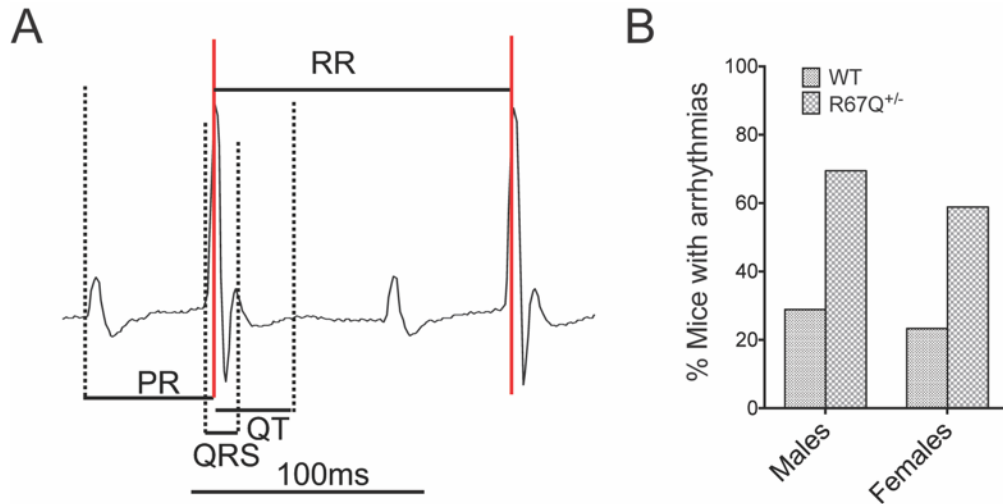
SUPPLEMENTAL MATERIALTable S1. *Echocardiographic assessment of cardiac function in R67Q^{+/-} mice*

Measurement	WT	R67Q ^{+/-}
Sex	4M/3F	6M/2F
LVID (d) (mm)	4.1 ± 0.1	3.9 ± 0.2
LVID (s) (mm)	3.0 ± 0.2	2.9 ± 0.3
LVPW (d) (mm)	0.6 ± 0.02	0.6 ± 0.02
LVPW (s) (mm)	0.8 ± 0.1	0.8 ± 0.1
% Ejection Fraction	52.6 ± 5.9	51.6 ± 6.4
Stroke Volume (μL)	27.4 ± 3.1	25.6 ± 3.4
Cardiac Output (ml/min)	12.6 ± 1.8	13.1 ± 2.4
% Fractional Shortening	37.5 ± 3.3	37.0 ± 0.7
LV Mass (mg)	79.1 ± 2.4	82.4 ± 7.4
LV Mass/B.W. (mg/g)	3.4 ± 0.1	3.5 ± 0.3
LV Volume; d (μL)	63.7 ± 3.6	52.1 ± 7.2
LV Volume; s (μL)	20.8 ± 4.1	16.7 ± 2.2
Heart Rate (bpm)	475 ± 20	486 ± 39

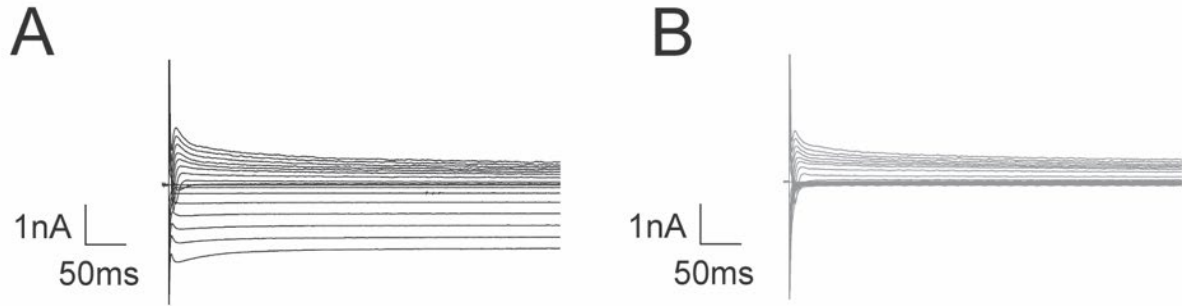
LV, left ventricle; *d*, diastole; *s*, systole; *B.W.*, body weight.



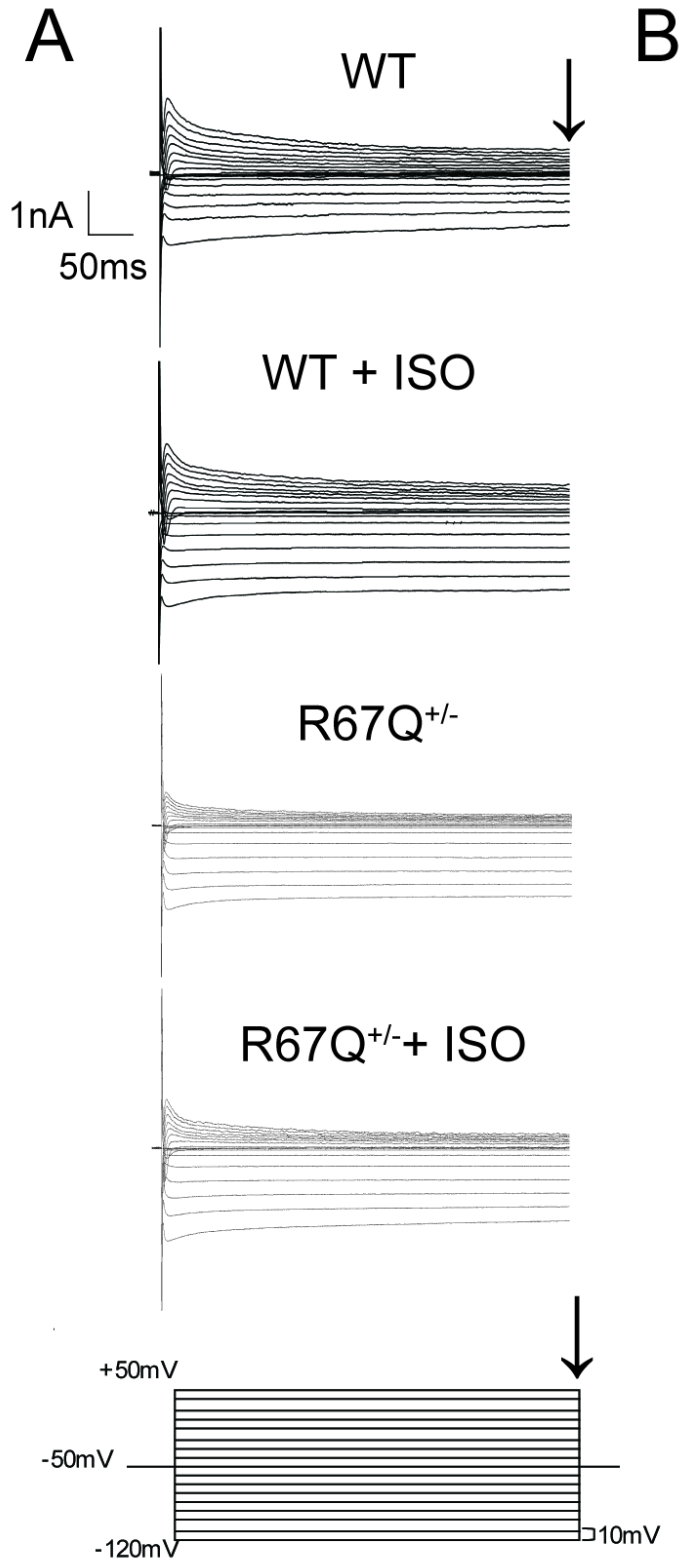
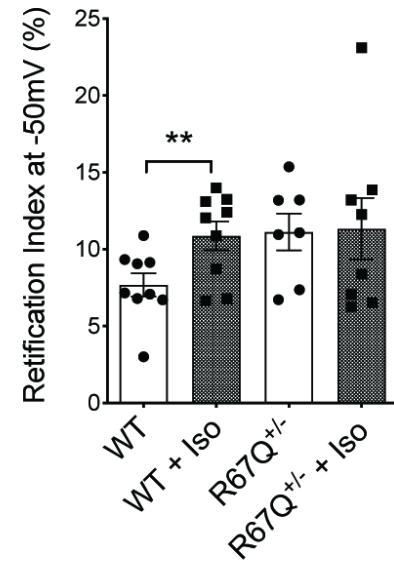
Supplemental Figure 1: Cardiac-specific gene targeting and mouse generation. **A.** Schematic detailing gene targeting in R67Q^{+/-} mice. A neocassette was inserted into the primary sequence of Kir2.1, flanked by loxP sites. The resultant mice from this targeting were then crossed with mice expressing Cre recombinase under the control of the α -MHC6 promoter ((B6.FVB-Tg(Myh6-cre)2182Mds/J). **B.** Representative PCR results from whole heart genotyping. Left panel (top and bottom) shows PCR results for Cre recombinase, right panel details PCR results for R67Q-*KCNJ2*. Presence of single band indicates negative for the gene of interest double band indicates positive for the gene of interest. Numbers above lanes indicate mouse number. **C.** Representative western blot from brain, heart and skeletal muscle. Kir2.1 expression is comparable between tissues, despite 1 allele being silenced due to non-excision of the neocassette in R67Q^{+/-} in the absence of Cre recombinase.



Supplemental Figure 2: R67Q^{+/-} Have Higher Incidence of Ventricular Arrhythmia in Response to Adrenergic Stress Compared to WT Mice. **A.** Schematic of criteria for analysis of ECG complexes. **B.** Development of any type of ventricular arrhythmia in response to adrenergic stress is not sex dependent, with both sexes in WT and R67Q^{+/-} having similar arrhythmic responses.



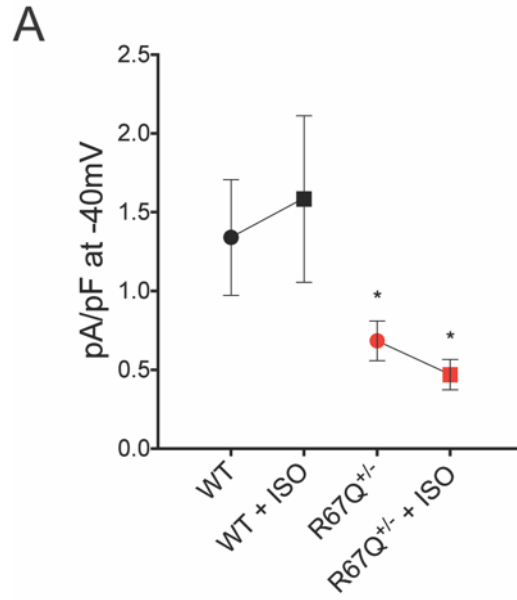
Supplemental Figure 3: IK1 current is sensitive to barium. A. Representative trace from WT myocyte in response to step protocol (see methods for description). **B.** Representative trace from same cell following perfusion of 0.5mM Barium Chloride for 2 minutes in response to same step protocol.

**B**

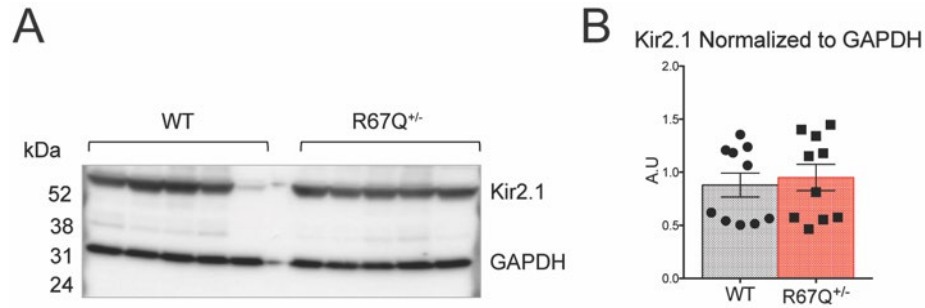
Supplemental Figure 4: Representative I_{K1} traces from WT and R67Q^{+/-} at baseline and response to ISO.

A. Representative current traces from WT (top), WT + isoproterenol (middle top), R67Q^{+/-} (middle bottom), and R67Q^{+/-} + isoproterenol (bottom). Schematic of the protocol is shown below the traces. Scale bar represents 50 ms and 1 nA/pF. IV relationships were measured at time indicated by arrow, approximately 500ms.

B. Rectification index of I_{K1} I-V relationships at -50mV. Rectification index was calculated as follows: This index was defined as the ratio of the outward current at -50 mV divided by the absolute value of the inward current at -100 mV and then multiplied by 100%. Rectification is significantly increased in WT following ISO, whereas was not affected by ISO in R67Q^{+/-} and was not significantly different from WT. ** - $p < 0.01$ by one-way repeated measures ANOVA with post-hoc Bonferroni correction was used.

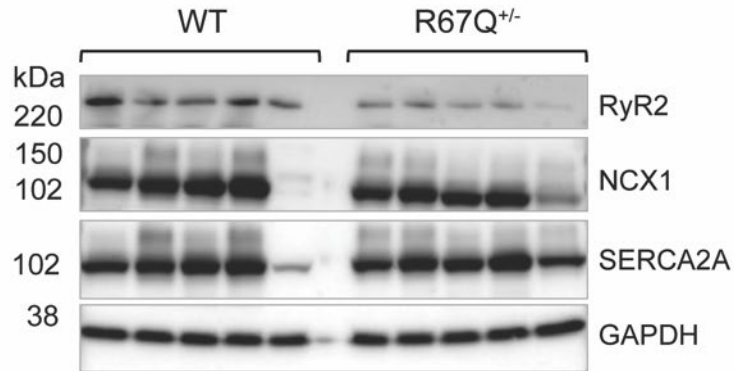


Supplemental Figure 5: R67Q^{+/-} ventricular myocytes have less I_{K1} at -40mV following ISO compared to WT. A. Absolute outward current values at -40mV in WT (1.34 ± 0.37 pA/pF) and R67Q^{+/-} (0.68 ± 0.13 pA/pF) at baseline. R67Q^{+/-} myocytes have significantly less outward current (0.47 ± 0.10 pA/pF) following ISO compared to WT (1.58 ± 0.53 pA/pF). Two-way repeated measures ANOVA with post-hoc Bonferroni correction was used.

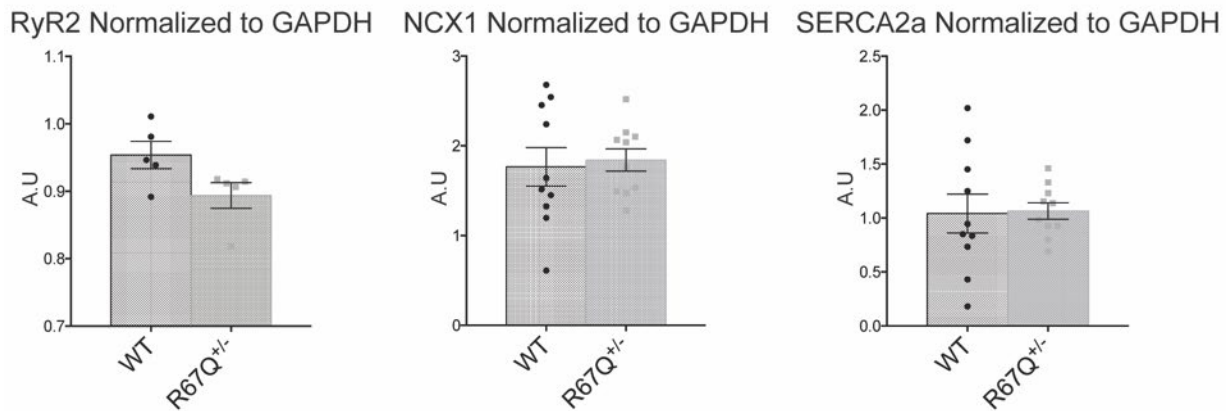


Supplemental Figure 6: Kir2.1 Expression is not significantly different between WT and R67Q^{+/-}. **A.** Representative western blot with expression levels of Kir2.1 and GAPDH from whole heart lysates from WT and R67Q^{+/-}. **B.** Western blot analysis revealed no significant difference in Kir2.1 protein expression between WT (1.04 ± 0.04 Arbitrary Units (A.U)) and R67Q^{+/-} (1.02 ± 0.09 A.U.) when normalized to GAPDH ($p > 0.1$). (N=4).

A

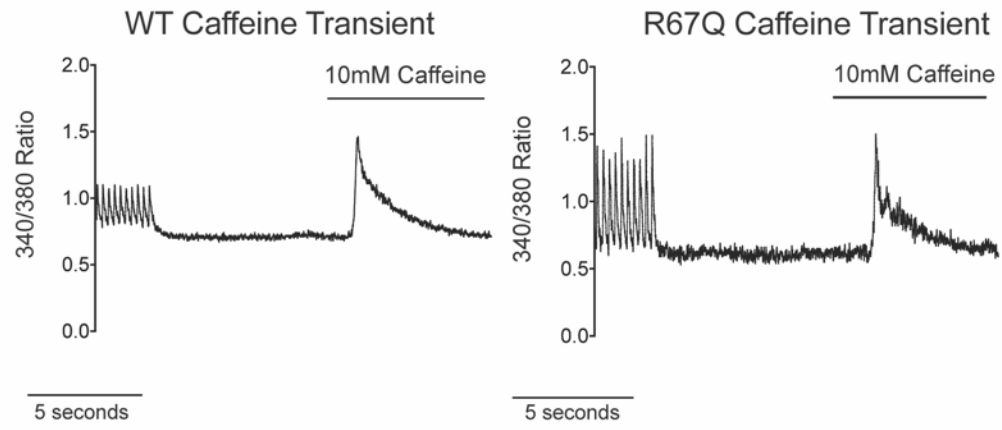


B

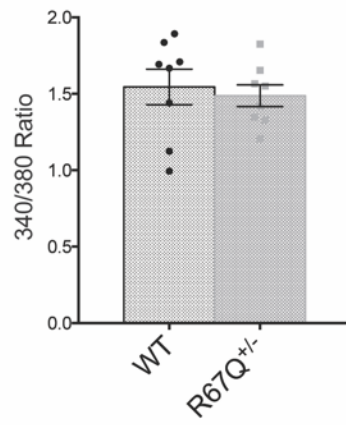


Supplemental Figure 7: Western blot analysis calcium handling proteins. A. Representative western blots of whole heart lysates. **B.** RyR2, NCX1 and SERCA2a protein expression was not significantly different between WT and R67Q^{+/-} whole heart lysates when normalized to GAPDH. Student's t-test was used to determine significance.

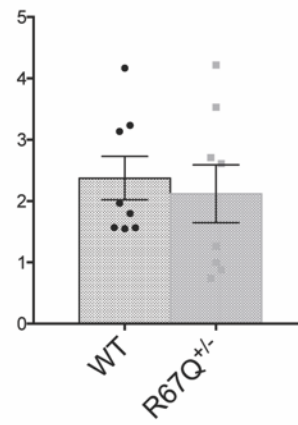
A



B



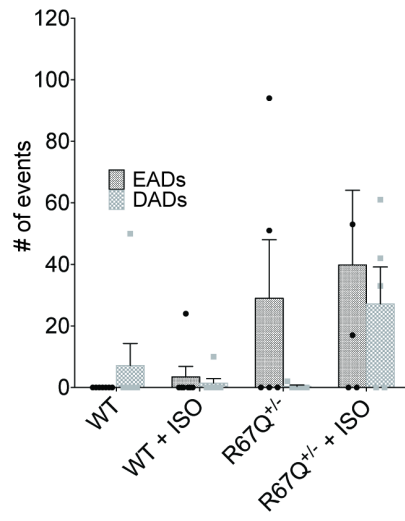
C



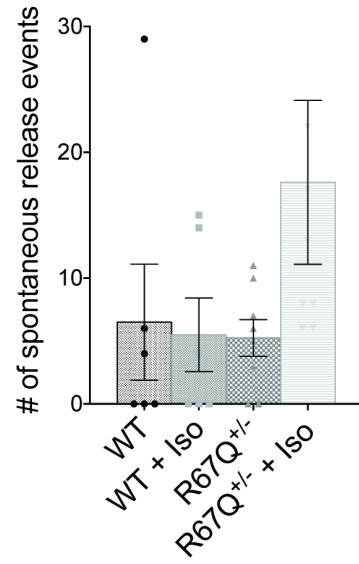
Supplemental Figure 8: R67Q^{+/-} does not impact SR Ca²⁺ handling. A.

Representative caffeine-elicited calcium transient from WT and R67Q^{+/-} myocytes. Cells were paced for 30 s at 2 Hz then pacing stopped, followed by application of 10 mM caffeine. **B.** Caffeine-evoked total Ca²⁺ release was comparable between WT and R67Q^{+/-} cells. **C.** Caffeine-evoked calcium transient decay was similar between WT and R67Q^{+/-} cells suggesting NCX1 activity was not adversely affected by the presence of the mutation. Students t-test was used to determine significance.

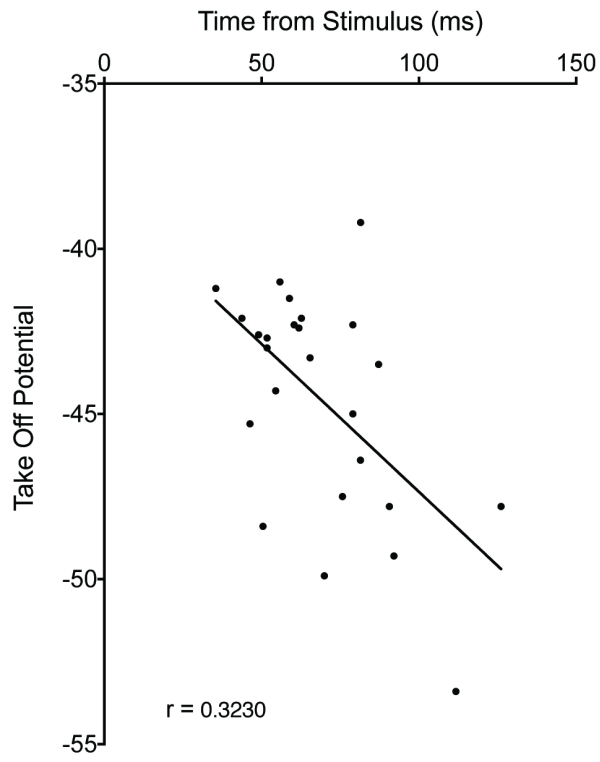
A



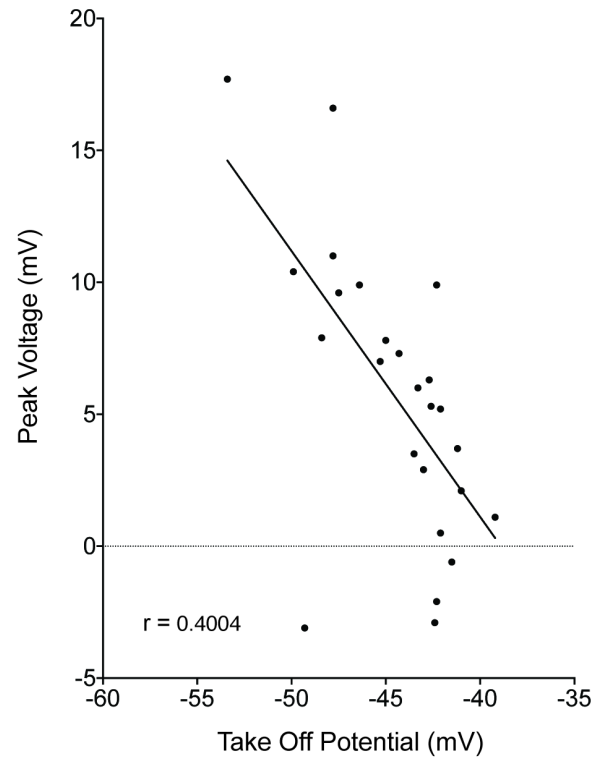
B



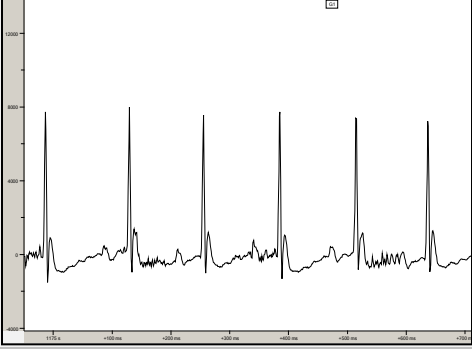
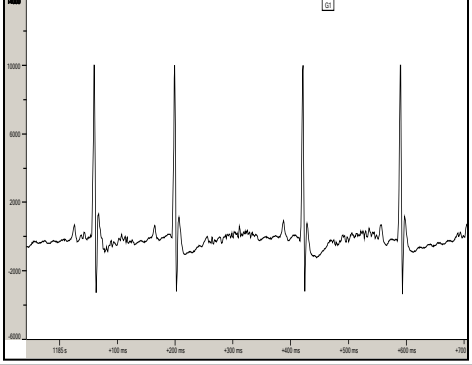
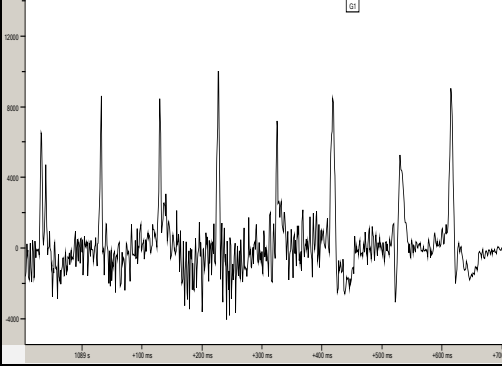
C

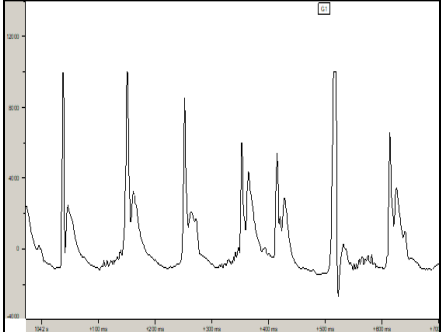
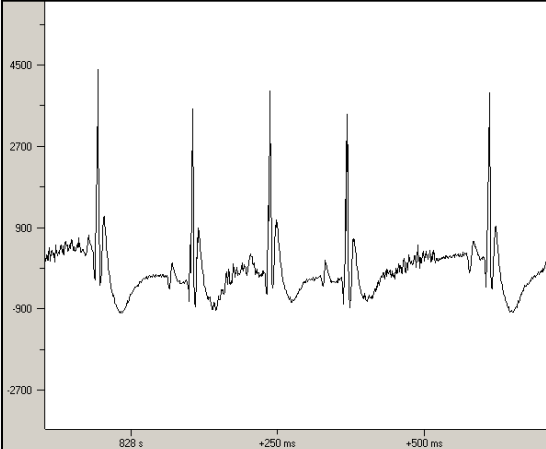
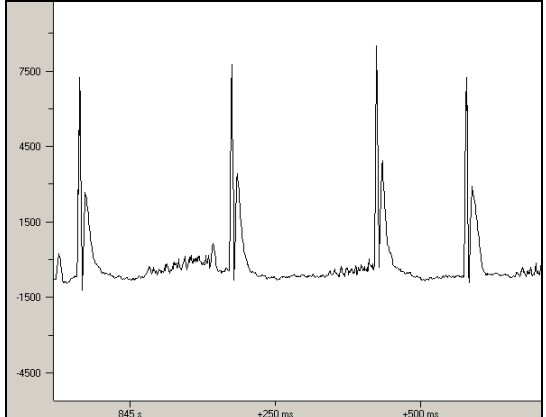


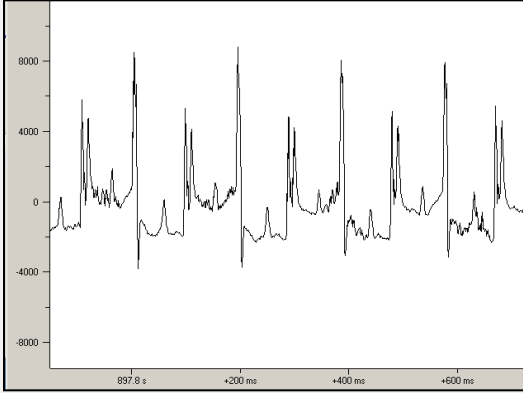
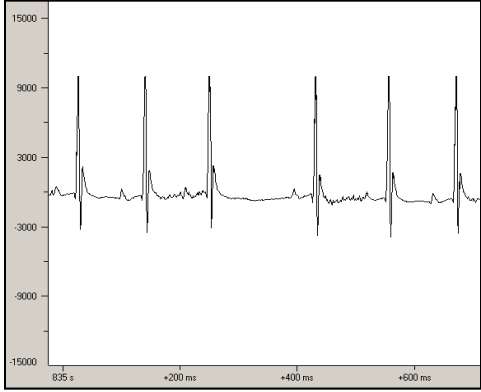
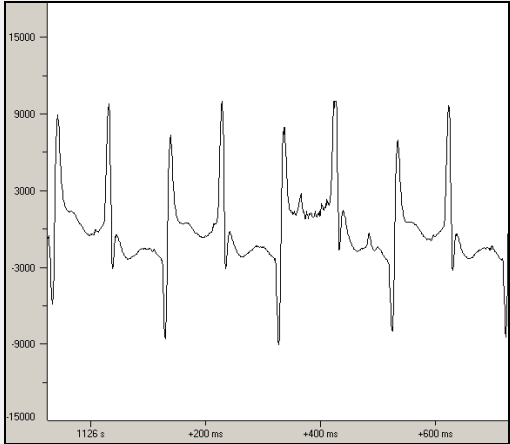
D



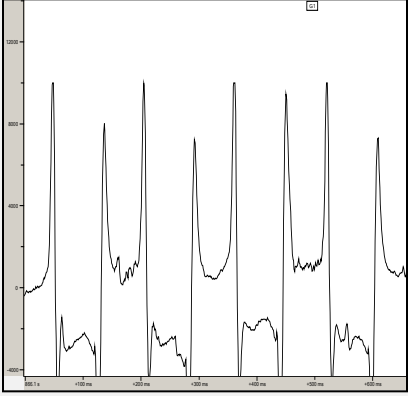
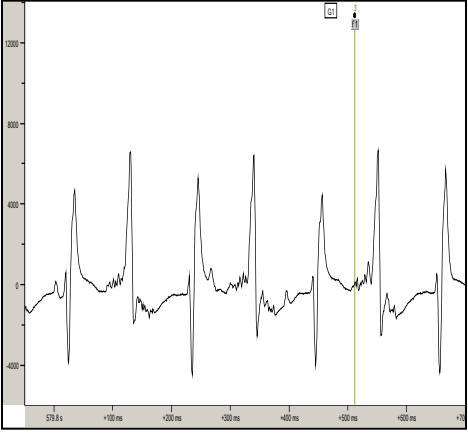
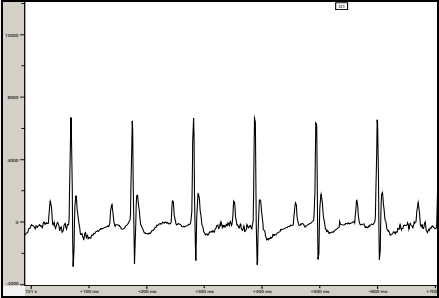
Supplemental Figure 9: R67Q^{+/-} Have More EADs than WT VMs Following ISO at 6Hz pacing. **A.** R67Q^{+/-} VMs developed more EADs following ISO compared to WT. Occurrence of DADs was also significantly increased in R67Q^{+/-} compared to WT during current clamp experiments. **B.** R67Q^{+/-} VMs had more spontaneous calcium release events compared to WT following ISO during calcium transient measurement experiments. **C.** Analysis of take off potential revealed depolarized potential compared to classical phase 2 EADs with delayed onset from stimulus. **D.** Take off potential vs peak voltage reached by phase 3 EADs in R67Q^{+/-} VMs. (WT - N=5, n=7; R67Q^{+/-} - N=4, n=10). Two-way repeated measures ANOVA with post-hoc Bonferroni correction (S8A and S8B) or non-linear regression (S8C and S8D) was used.

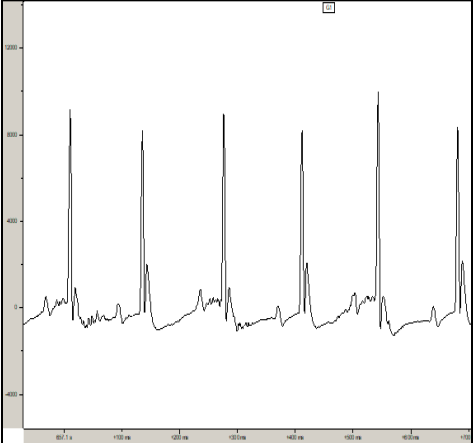
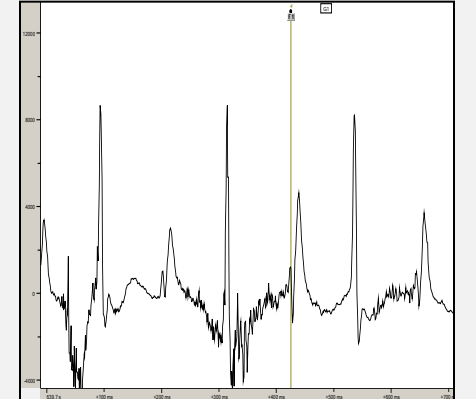
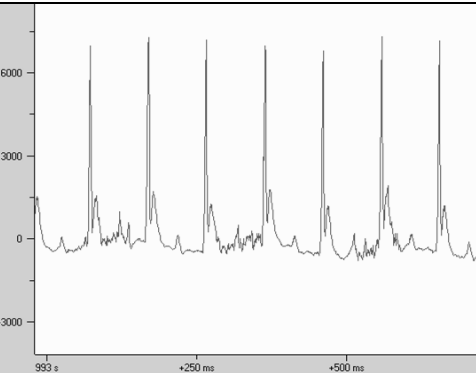
Animal #	Genotype	Baseline Rhythm	Rhythm Post-IP	Representative ECG
654	R67Q ^{+/-}	Sinus	Sinus Tach	
655	R67Q ^{+/-}	Sinus	Sinus Tach	
708	R67Q ^{+/-}	Sinus	Bi-VT	

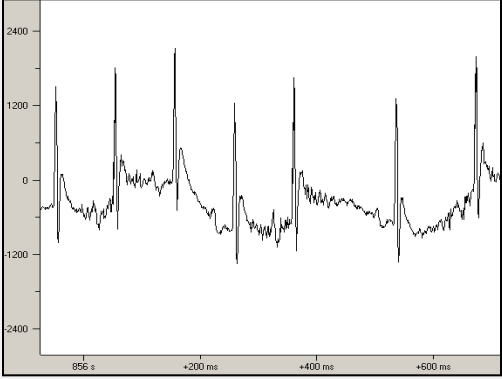
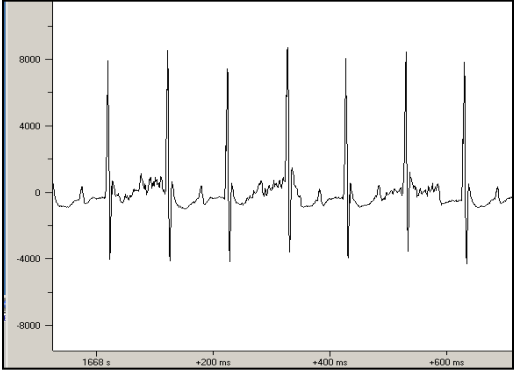
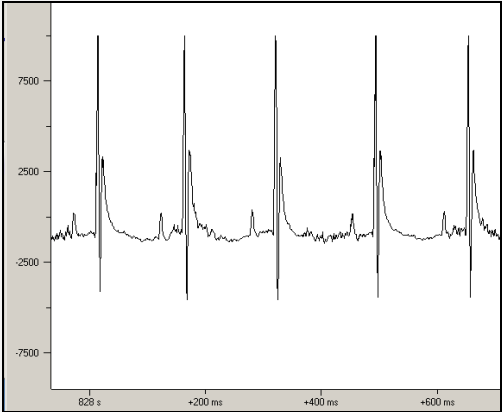
724	R67Q ^{+/-}	Sinus	PMVT	 <p>ECG trace showing sinus rhythm with PMVT (Premature Ventricular Motion) in R67Q^{+/-} mouse. The trace displays regular sinus beats with occasional premature, wide QRS complexes.</p>
526	R67Q ^{+/-}	Sinus	Sinus With Pause + PVC	 <p>ECG trace showing sinus rhythm with a pause and a PVC (Premature Ventricular Complex) in R67Q^{+/-} mouse. The trace shows a regular sinus rhythm with a significant pause followed by a premature, wide QRS complex.</p>
532	R67Q ^{+/-}	Sinus	Sinus With PVCs	 <p>ECG trace showing sinus rhythm with PVCs (Premature Ventricular Complexes) in R67Q^{+/-} mouse. The trace displays regular sinus beats with occasional premature, wide QRS complexes.</p>

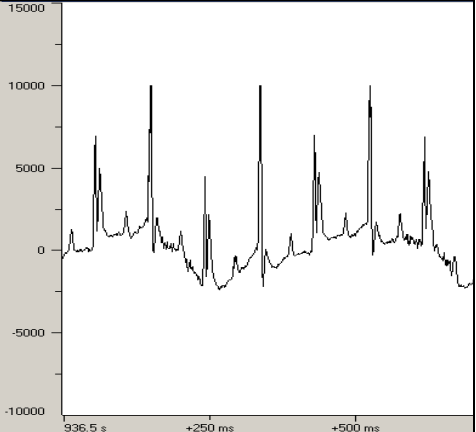
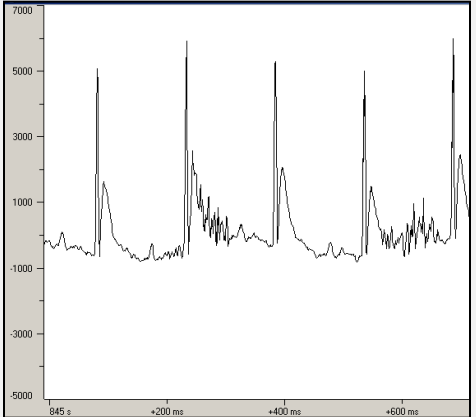
541	R67Q ^{+/-}	Sinus	Sinus With Ventricular Bigeminy	
547	R67Q ^{+/-}	Sinus	Sinus With PAC	
608	R67Q ^{+/-}	Sinus	Bi-VT	

<p>612</p>	<p>R67Q^{+/-}</p>	<p>Sinus</p>	<p>Sinus Tach</p>	
<p>616</p>	<p>R67Q^{+/-}</p>	<p>Sinus</p>	<p>Sinus Tach With PVC In Trigeminy</p>	
<p>630</p>	<p>R67Q^{+/-}</p>	<p>Sinus</p>	<p>Sinus Tach</p>	

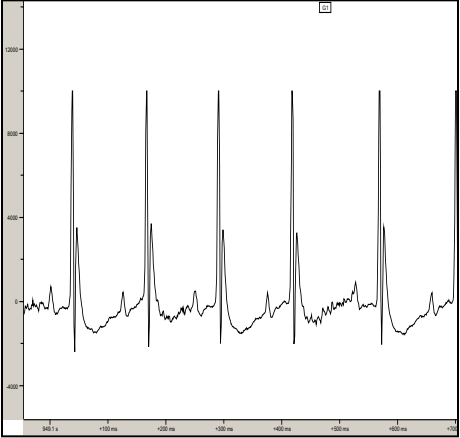
749	R67Q ^{+/-}	Sinus	Bi-VT	
854	R67Q ^{+/-}	Sinus	Bi-VT	
860	R67Q ^{+/-}	Sinus	Sinus Tach	

865	R67Q ^{+/-}	Sinus	Sinus Tach	
867	R67Q ^{+/-}	Sinus	Bi-VT	
525	WT	Sinus	Sinus/Sinus Tach	

529	WT	Sinus	Sinus/Sinus Tach	
546	WT	Sinus	Sinus	
548	WT	Sinus	Sinus Tach	

609	WT	Sinus	Sinus Tach	
613	WT	Sinus	Sinus Tach	

729	WT	Sinus	Sinus	
861	WT	Sinus	Sinus	

862	WT	Sinus	Sinus		
864	WT	Sinus	Sinus Tach	